Data Supplement for Doucet et al., The Role of Intrinsic Brain Functional Connectivity in Vulnerability and Resilience to Bipolar Disorder. Am J Psychiatry (doi: 10.1176/appi.ajp.2017.17010095)

Contents

Sample Recruitment and Assessment. We analyzed three groups of participants: patients with bipolar I disorder (BD, n=78); unaffected siblings of patients with BD-I (SIB, n=64); and healthy volunteers (HV, n=41). All diagnoses were determined by personal interview using the Structured Clinical Interview (SCID) for the Diagnostic and Statistical Manual of Mental Disorders-IV (DSM-IV) (1) (patients or non-patient edition as indicated). IQ was assessed using the Wechsler Abbreviated Intelligence Scale (2). Current mood symptoms were measured using the Hamilton Depression Scale (HAMD) (3), the Young Mania Rating Scale (YMRS) (4) and the expanded version of the Brief Psychiatric Rating Scale (BPRS) (5). Forty-three of the siblings were related to the patients. The extended Brief Psychiatric Rating Scale (BPRS) is a 24-item scale that covers a wide range of symptoms. The absence of a symptom is rated as 1. Therefore, if all symptoms are absent the score is 24.

Eligibility criteria for patients: (a) BD-I diagnosis; (b) no history of major medical or neurological conditions (e.g. epilepsy, migraine, head trauma with loss of consciousness); (c) IQ > 80; d) in remission as defined by DSM-IV; (d) had no current substance or alcohol abuse/dependence; substance use, but not dependence, was allowed if participants had been abstinent for a minimum of 3 months. Among the BD patients, 23% had a history of psychosis, whereas 77% of them had never experienced any psychotic symptoms. However, having a history of psychosis did not significantly affect psychiatric measures among the patients or among the siblings of patients with a history of psychosis.

Eligibility criteria for healthy participants (siblings and unrelated volunteers): (a) no current or lifetime diagnosis of any disorder in the bipolar or schizophrenia spectrum; (b) no history of medical or neurological conditions; (c) IQ>80; and d) had no current substance or alcohol abuse/dependence; substance use, but not dependence, was allowed if participants had been abstinent for a minimum of 3 months. In addition, healthy unrelated volunteers were enrolled only if they had no family history of psychotic or mood disorders as reported by detailed family history.

Neuroimaging

MRI Acquisition. All scans were collected at the Olin Neuropsychiatry Research Center, Institute of Living/Hartford Hospital using a research dedicated Siemens Allegra 3T scanner. A total of 5 minutes 15 seconds of a resting state condition was collected utilizing Bold Oxygen

Level Dependent signal. Anatomical and resting state acquisitions were identical for all participants. A single shot echoplanar gradient echo imaging sequence acquiring T2* signal was used with the following parameters: 210 volumes, 29 axial slices acquired parallel to the AC-PC line, TR=1.5s, TE=27ms, field of view=24*24cm, acquisition matrix=64*64, flip angle=60°, voxel size=3.43*3.43*5mm). The in-plane resolution was 3.4*3.4mm^2 with a slice thickness of 5 mm. Subjects lay in a foam pad to comfortably stabilize the head, were instructed to remain still throughout the scan, not fall asleep, and keep their eyes open during the entire scan. Structural images were acquired using a T_1-weighted, 3D magnetization-prepared rapid gradient-echo (MPRAGE) sequence (TR/TE/TI = 2200/4.13/766 ms, flip angle = 13°, voxel size [isotropic] = 0.8 mm, image size = 240*320*208 voxels), with axial slices parallel to the AC-PC line. To increase signal-to-noise ratio, four volumes were acquired per subject.

MRI Preprocessing. Data from the participants were preprocessed identically using SPM12 (http://www.fil.ion.ucl.ac.uk/spm/software/spm12). A six-parameter variance cost function rigid body affine registration was used to realign all images within a session to the first volume. Motion regressors were computed and later used as regressors of no interest. To maximize mutual information, coregistration between the functional scans and the average anatomical T1 scan was carried out using six iterations and resampled with a 7th-Degree B-Spline interpolation. Functional images were then normalized into standard space (MNI305) to allow for signal averaging across subjects. We utilized the standard normalization method in SPM12, which minimizes the sum-of-squared differences between the subject's image and the template (MNI305), while maximizing the prior probability of the transformation. The segmentation of the data in to gray matter, white matter (WM), and cerebro-spinal fluid (CSF) classes was then completed. All normalized images were smoothed by convolution with a Gaussian kernel, with a full width at half maximum of 6 mm in all directions. Sources of spurious variance were then removed from the data through linear regression: six parameters obtained by rigid body correction of head motion, the CSF and WM signals. For each individual, the time-courses of both WM and CSF were estimated in the relevant brain tissue classes defined at the segmentation step. Finally, fMRI data were temporally filtered using the REST Toolbox (low cutoff frequency = 0.01 Hz – high cutoff frequency 0.08 Hz) (8, 9).

Head Motion:

For each individual, the average six maximal volume-to-volume head movement was less than 1 (degree or mm). The groups did not differ in any direction (Table S1).

TABLE S1. Averaged maximal volume-to-volume head movement in each direction for each group

Direction	Patients with Bipolar Disorder	Siblings	Healthy Volunteers	p-value*
Axial	0.2818	0.1697	0.2097	0.06
Coronal	0.3576	0.3114	0.3991	0.46
Sagittal	0.5874	0.4874	0.5856	0.38
Rotation 1	0.0088	0.0088	0.0083	0.97
Rotation 2	0.0033	0.0022	0.0033	0.15
Rotation 3	0.004	0.0022	0.0027	0.09

*: p-value uncorrected for multiple comparisons

Exclusion of regions of interest with loss of signal: The gray matter areas were initially defined using automated anatomical labeling (10) and then subdivided into 638 finer regions with approximately similar size (11, 12); no regional parcel crossed the midline between hemispheres or lobar boundaries within hemispheres. Individual signal-to-noise ratio (SNR) was estimated after motion correction and averaged over voxels for each gray matter region. The regions with a consistent low SNR (e.g. less than 2 standard-deviations from average brain signal) along the full sample were excluded from network analyses (Figure S1). Thus, 18 regions were excluded from consideration, mostly in the ventral and inferior temporal areas that are frequently compromised by susceptibility artifact, resulting in a total of 620 regions.

V. Computation of Global and Regional Measures: This study used several metrics to estimate the topological properties of the brain at rest. Degree and participation coefficient were estimated at each node (brain region). Nodal clustering and efficiency were averaged over nodes to estimate global clustering and global efficiency. Small-worldness and characteristic path length were also estimated at the whole brain level.

The **nodal degree** is equal to the number of links connected to that node. It can be expressed as:

$$K_i = \sum a_{ij},$$

where a_{ij} is the connection status between node *i* and node *j*.

The **participation coefficient** assesses the diversity of intermodular interconnection of individual nodes. It represents the diversity of regional connections between distinct subnetworks (13). Nodes with a high participation coefficient are referred to as connector hubs

and are likely to facilitate global intermodular integration. The participation coefficient can be expressed as:

$$y_i = 1 - \sum_{m \in M} \left(\frac{K_i(m)}{K_i} \right)^2,$$

where *M* is the set of modules, and $K_i(m)$ is the number of links between the node *i* and all nodes in module *m*.

The **clustering coefficient** of the whole brain can be defined as the average fraction of all possible edges realized around a node. It is a measure of segregation, and can be defined as:

$$C = \frac{1}{n} \sum_{i \in N} \frac{2t_i}{K_i(K_i - 1)},$$

where t_i is the number of triangles around a node *i,* and *N* is the number of nodes in the network.

The **global efficiency** is a measure of the propensity of the network to be globally interconnected and it is computed as the average inverse shortest path length between all pairs of regions (14). It is commonly referred to as a measure of network integration. In other words, it can be used to quantify the extent to which nodes communicate with distant nodes, and theoretically predicts the efficacy of information exchange throughout the entire network. The global efficiency can be expressed mathematically as:

$$E_{glob} = \frac{1}{N(N-1)} \sum_{i=1}^{N} \sum_{j \neq i}^{N} \frac{1}{L_{min}(i,j)},$$

where $L_{min}(i,j)$ denotes the shortest path length between node *i* and node *j*, and *N* is the number of nodes in the network.

The **characteristic path length** is the average shortest path length to all other nodes. A small characteristic path length is a sign of long paths, and therefore reduced integration. It can be expressed as:

$$L = \frac{1}{n} \sum_{i \in N} \frac{\sum_{j \in N, j \neq i} d_{ij}}{n - 1},$$

where d_{ij} is the distance between node *i* and all other nodes.

The **small-worldness** represents a balance between functional segregation and integration in a network. Small-world networks are defined as networks that are significantly more clustered than a random network while maintaining a path length similar to a random network ($e.g., \sigma > 1$). This measure can be expressed as:

$$\sigma = \frac{C/C_R}{L/L_R},$$

where C_R and L_R are the clustering coefficient and the characteristic path length of a random graph, respectively. The variables C_R and L_R were estimated based on 100 random graphs (15). Random graphs are characterized by very high global efficiency, but very low clustering coefficients, reflecting a perceived imbalance between integration and segregation.

To compute each measure, a set of thresholds was applied, producing a series of binarized matrices. The fixed thresholds ranged from 1% to 50% of all connections, in increments of 1%. Negative correlations were set to zero. The measures were estimated using MATLAB code in the Brain Connectivity Toolbox (15).

Network robustness was assessed by removing nodes (and corresponding connections) either in descending order of their nodal degree (targeted attack) or in random order (random error attack) (16). To do so, we incrementally increased the number of deleted nodes from 0 to 620 in increments of 1, and recalculated the global efficiency of the remaining network after deletion of each node (17). The area under the curve of normalized global efficiency (scaled to maximum) as a function of the percentage of deleted nodes was defined as a summary measure of the resilience of a network (18). This result is reported in Figure S2.

Computation of Mesoscale Measures (Brain Modularity): The individual (weighted) correlation matrices were used to identify groups of brain regions that were densely interconnected by strong functional connectivity, using modularity maximization (19). To do so, we utilized the Louvain-like locally greedy algorithm implemented in MATLAB. To identify an optimal partition of nodes into modules *m*, we searched for a partition that maximized the following modularity quality function:

$$Q = \sum_{ij \in N}(a_{ij} - \gamma * \frac{K_i K_j}{w})\delta_{m_i,m_j},$$

where m_i is the module containing node *i*, *w* is the sum of all weights, and $\delta_{m_i,m_j} = 1$ if node *i* and node *j* are in the same module and $\delta_{m_i,m_j} = 0$ otherwise.

Mathematically, it is known that increasing the resolution parameter ɣ yields increasingly smaller modules (20). While a resolution parameter ɣ value of 1 is the most common choice in the literature, we chose to gradually increase the resolution parameter ɣ from 0.5 to 1.5 (in intervals of 0.1) to test the reliability of the community structure.
This routine can return different results from run to run because it considers nodes in pseudorandom order (21). We therefore ran the modularity maximization function 100 times, and therefore, obtained 100 partitions, for each individual (20). In order to determine the most representative partition, we used an iterative thresholding procedure available in the Network Community Toolbox (http://commdetect.weebly.com) (22).

Additional analyses:

Effect of medication on connectivity: When a significant effect was revealed on a global or local measure between the BD and HV groups, we tested the effect of medication, computing a Kruskal-Wallis test with the medication type as a categorical variable (four classes were created based on patients' medication (See Table S1): no medication (n=15); one drug (n=17); two drugs (n=33); three or more drugs (n=12), within the patient group.
We found that there was no effect of medication load on the nodal degree that survived correction for multiple comparisons in the patients with BD.

Intra-Class correlation coefficient of connectivity measures between siblings and patients: To make sure that our local results involving SIB and patients with BD were not biased by their family relationship, we computed the intra-class correlation (ICC) on the significant metrics (nodal degree and participation coefficient) including the 43 siblings-patients pairs that were related. The results showed that, for the nodal degree, the maximal ICC was 0.38 while for the participation coefficient; the maximal ICC was 0.27. These values indicate poor relatedness of the metrics between the SIB and the patients (ICC<0.4) (23), suggesting that our results are unlikely caused by the existing familial relationship.

Clinical correlates of connectivity measures: We used two different approaches to investigate effects of the severity of symptoms. In the dimensional approach, we examined the Spearman's correlation between total scores of BPRS, HAMD and YPRS and any metrics for which the group effect was significant. We specified that only correlations above 0.3 would be considered as potentially biologically meaningful (24).

In the categorical analysis, we excluded patients with BPRS score over 40 (n=16) to ensure that any symptoms ratings were mild or absent and re-computed the graph-theory analyses to test for group effects. Conventionally, a BPRS score of approximately 30 corresponds to a Clinical Global Impression (CGI) rating of “mildly symptomatic”, a score of approximately 40 corresponds to a CGI rating of “moderately symptomatic” and scores of 53 or higher correspond to a CGI rating of “markedly symptomatic” (29).

The first type of analyses did not reveal meaningful correlations between the severity of psychopathology and the regional metrics in the patients.

When excluding individuals with BPRS above 40, no between-group differences were observed for the averaged clustering coefficient, the characteristic path length, the global efficiency, or the small-worldness.

When excluding individuals with BPRS above 40, the results remain approximately similar to those observed in the whole sample (N=183) for the nodal degree measure. The regions reflective of vulnerability to BD were mostly located in the pre- and post-central gyri, while the regions reflective of resiliency to BD were in the fusiform gyrus and the supplementary motor area. However, a region, not described when investigating the whole sample, was found as disease expression specific (lowest degree for BD than in the two other groups), located in the left middle occipital gyrus.

When excluding individuals with BPRS above 40, the results remain approximately similar to those observed in the whole sample (N=183) for the participation coefficient, although fewer regions showed significant between-group differences. The left hippocampus and the inferior temporal gyrus remain reflective of the disease expression (lowest participation for the BDs); while the left inferior frontal and right angular gyri remain reflective of resilience to BD (highest participation for the SIB).

Resilience in Siblings. Although siblings have about a 10-fold increase in risk compared to the general population, the prevalence of BD in these individuals is relatively low because the base prevalence of BD is also low. Goodwin and Jamison (6) reviewed the relevant studies and estimated the mean weighted prevalence of BD (all subtypes included) at 11.9% (page 416;

Table 13-2). If we apply this estimate to our sample, at most 8 of the siblings may convert to BD at some future point.

At present, it is not possible to provide personalized estimates of resilience and we would argue that the same applies to estimates of risk. Nevertheless, we conducted three additional analyses that address this issue. First, the peak incidence of BD is in the second decade of life and the risk of conversion drops significantly thereafter (e.g. (7)). We therefore divided the siblings group in those below (n=37) and above (n=27) the age of 30 years. The two subgroups did not differ in any demographic, cognitive (FSIQ) or imaging measures (modularity measures, functional connectivity) ($p>0.1$ for all). Moreover, they did not differ in any graph theory metric. Second, divided the siblings in those who had no lifetime psychopathology (n=44) and those (n=20) with positive personal psychiatric histories for non-BD disorders (substance use, anxiety disorders) (detailed in Table S1). Those with positive psychiatric history had higher HAMD scores ($p=0.01$, uncorrected) but did not differ in terms of the graph theory metric examined. Third, we repeated the analyses excluding all siblings with a personal psychiatric history and the results remained the same.

Permutation Testing. We ran 10,000 permutations, randomly selecting 50% of the sibling sample at each permutation. At each permutation we computed average nodal degrees and participation coefficients. We tested the null hypotheses comparing the distribution of the 10,000 permuted values to the value of the whole group. None of the tests were significant, even at an uncorrected *p*-value of 0.05 (minimum *p*-value=0.057 uncorrected, all *t*-values < 2).

Reliability Analyses. Because our results could be influenced by our choice of graph theory measures and anatomical parcellation, we addressed these issues by computing two additional analyses. First, the network-based statistic (NBS) toolbox (25) was used to identify the between-group differences in functional connectivity strength between all the 620 regions in our template, by applying a threshold of $t \geq 3.5$ to form a set of suprathreshold connected clusters evaluated statistically using permutation testing (5,000 permutations). This method does not involve any graph theory measures or modularity patterns. We found consistent results with our major findings as seen in Figure S6A.

Second, we used the functional parcellation provided by the Functional Imaging in Neuropsychiatric Disorders Lab (http://findlab.stanford.edu/) (26). We then applied a dual

regression to identify networks in each individual and computed t-tests between the groups. Significant differences between groups were reported at $p<0.001$ (uncorrected, $k>10$, based on the number of voxels expected per cluster). As displayed on Figure S6B, the results remained identical, revealing reduced connectivity within the SMN in both patients with BD and SIB, relative to the HV group.

These additional analyses confirm that our results are independent of anatomical parcellation and the method for assessing connectivity.

The software R-cran was used to compute statistics (27). The nodal topological measures and networks are visualized with the BrainNet Viewer (http://www.nitrc.org/projects/bnv/) (28).

TABLE S2. Group differences in nodal degree

N region (Atlas)[a]	Region	Network	BD diff HV	BD diff SIB	SIB diff HV	Cohen d BD / HV	Cohen d BD / SIB	Cohen d SIB / HV
39	L IFG	CEN	0.028	0.084	0.282	0.37		
120	R MFG	CEN	0.005	0.034	0.249	0.48	0.31	
153	L Superior MPFC	DMN	0.009	0.421	0.032	0.45		0.37
155	L Superior MPFC	CEN	0.023	0.458	0.055	0.38		
156	L superior MPFC	DMN	0.016	0.089	0.266	0.41		
168	R Superior MPFC	CEN	0.027	0.502	0.042	0.36		0.34
198	L Fusiform	VN	0.253	0.028	0.156		0.32	
205	R Fusiform	VN	0.409	0.025	0.042		0.32	0.35
208	R Fusiform	VN	0.170	0.036	0.288		0.31	
211	R ITG	DMN	0.018	0.042	0.257		0.17	
213	R Fusiform	VN	0.293	0.013	0.114		0.37	
290	R SOG	VN	0.020	0.244	0.133	0.39		
372	L Postcentral	SMN	0.298	0.054	0.039			0.36
373	L Postcentral	SMN	0.124	0.159	0.043	0.21		0.35
393	R Postcentral	SMN	0.128	0.199	0.043			0.33
405	L Precentral	SMN	0.143	0.097	0.030			0.38
407	L Precentral	SMN	0.117	0.060	0.014	0.22		0.43
412	R Postcentral	SMN	0.214	0.072	0.032			0.37
413	R Precentral	SMN	0.037	0.348	0.034	0.34		0.37
415	R Postcentral	SMN	0.464	0.037	0.073		0.30	
421	R Precentral	SMN	0.205	0.094	0.049			0.33
424	R Precentral	SMN	0.020	0.250	0.009	0.39		0.47
482	L SMA	SMN	0.343	0.019	0.111		0.33	
483	L SMA	SMN	0.006	0.138	0.113	0.46		
484	L SMA	DMN	0.004	0.176	0.065	0.53		
494	R SMA	CEN	0.015	0.028	0.294	0.43	0.32	
507	R SMG	SMN	0.003	0.145	0.074	0.55		
512	R SMG	CEN	0.009	0.065	0.247	0.45		
513	L ITG	DMN	0.022	0.449	0.052	0.23		
517	L ITG	DMN	0.008	0.050	0.190	0.30		
559	L ITG	DMN	0.095	0.195	0.042			0.34
625	R Caudate	CEN	0.012	0.406	0.019	0.41		0.41

The significant regions are defined based on the FDA approach ($p<0.05$; 5,000 iterations). [a]: Region Number in the 638 region atlas. The value represents the p-value of the true group difference, defined as the number of times the random curve values were greater than the true curve value, divided by the number of iterations. The shaded boxes reveal p-value below 0.05. Abbreviations: DMN: Default mode network, CEN: Central executive network, ITG: Inferior temporal gyrus, L: left, MFG: middle frontal gyrus, MOG: middle occipital gyrus, MPFC: medial prefrontal cortex, SMA: supplementary motor area, SMN: Sensorimotor network, SOG: Superior occipital gyrus, R: right, SMG: supramarginal gyrus, VN: Visual network.

TABLE S3. Group differences in participation coefficient

N region (Atlas)[a]	Region	**Network**	**BD diff HV**	**BD diff SIB**	**SIB diff HV**	Cohen d BD / HV	Cohen d BD / SIB	Cohen d SIB / HV
145	L MPFC	DMN	0.044	0.184	0.163	0.35		
166	R MPFC	DMN	0.046	0.032	0.486	0.41	0.42	
218	L Hippocampus	DMN	0.044	0.060	0.397	0.55		
243	L Lingual	VN	0.049	0.168	0.014	0.28		0.61
320	L paracentral	SMN	0.010	0.430	0.012	0.44		0.68
410	L Precentral	SMN	0.024	0.407	0.013	0.39		0.68
53	L IFG	DMN	0.359	0.039	0.030		0.63	0.65
200	L Fusiform	DMN	0.203	0.022	0.203		0.52	
271	L MOG	VN	0.161	0.102	0.037			0.49
295	R Angular	DMN	0.229	0.050	0.017		0.51	0.52
296	R Angular	DMN	0.436	0.011	0.019		0.51	0.48
307	L ventral ACC	DMN	0.258	0.043	0.031		0.47	0.47
308	R ventral ACC	DMN	0.351	0.032	0.043		0.37	0.32
314	L PHG	DMN	0.263	0.024	0.162		0.55	
432	L Precuneus	DMN	0.390	0.050	0.051		0.40	
444	R Precuneus	DMN	0.063	0.311	0.049			0.53
499	R SMA	SMN	0.144	0.072	0.017			0.72
513	L ITG	DMN	0.305	0.035	0.141		0.42	
519	L ITG	DMN	0.090	0.037	0.420		0.52	
562	L MTG	DMN	0.364	0.017	0.112		0.60	
580	R ITG	DMN	0.108	0.043	0.403		0.44	
583	L Temporal Pole	DMN	0.331	0.047	0.150		0.51	
589	R Temporal Pole	DMN	0.444	0.021	0.058		0.55	

The significant regions are defined based on the FDA approach ($p<0.05$; 5,000 iterations). [a]: Region Number in the 638 region atlas. The value represents the p-value of the true group difference, defined as the number of times the random curve values were greater than the true curve value, divided by the number of iterations. The shaded boxes reveal p-value below 0.05.

Abbreviations: ACC: anterior cingulate cortex, DMN: Default mode network, CEN: Central executive network, IFG: inferior frontal gyrus, ITG: Inferior temporal gyrus, L: left, MPFC: medial prefrontal cortex, MOG: middle occipital gyrus, MTG: middle temporal gyrus, PHG: parahippocampal gyrus, R: right, SMN: Sensorimotor network, VN: Visual network.

FIGURE S1. Description of the 18 regions excluded caused by loss of signal.

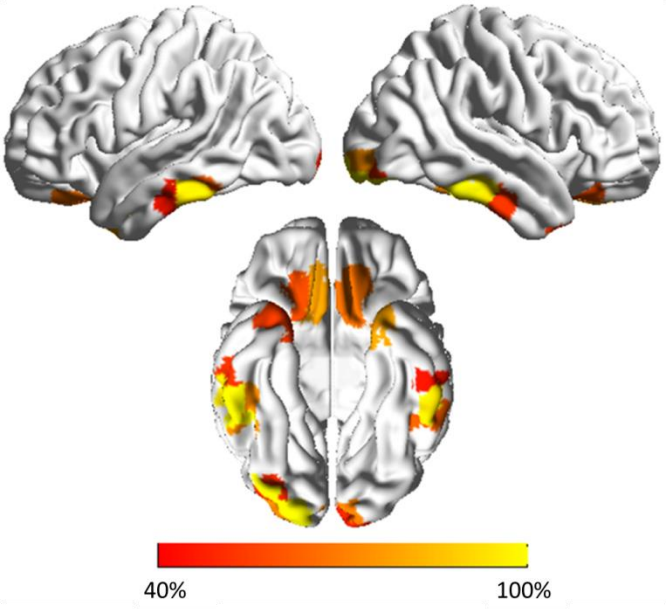

The figure shows the percentage of participants having significant loss of signal (more than 2 standard-deviations from average brain signal) in each of the 18 regions.

FIGURE S2. Network robustness to targeted and random attack, as a function of connection density.

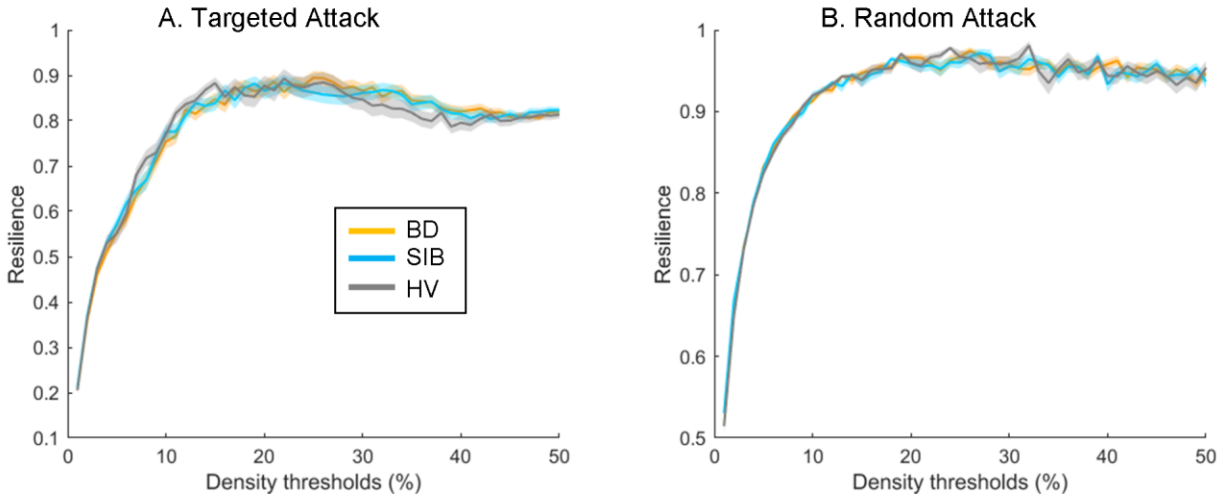

No significant differences were revealed between the groups ($p<0.05$, False Discovery Rate corrected). Confidence intervals on the curves represent 1 standard error. BD=patients with Bipolar Disorder; SIB=siblings; HV=healthy volunteers.

FIGURE S3. Violin plots showing within- and between-module functional connectivity for each group

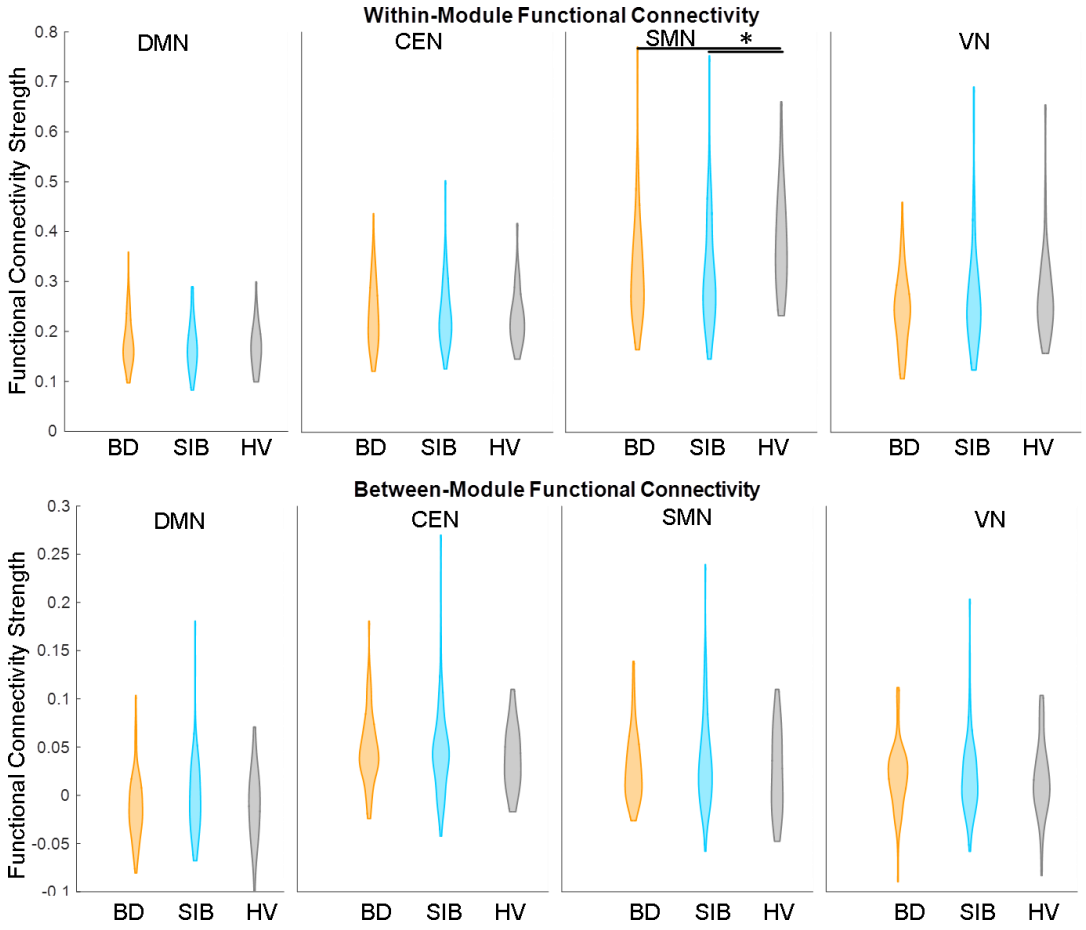

Resolution parameter equal to 1.* indicates significant effect between the healthy volunteers and the two other groups (Kruskal Wallis post-hoc; patients: H=-31.9, p=0.005; siblings: H=-35.8, p=0.002). The bar level displays mean of the sample while the points show the distribution of the sample. Orange = Patients with Bipolar Disorder, blue = Siblings, grey = Healthy Volunteers.

FIGURE S4. Local topological differences between BD and SIB.

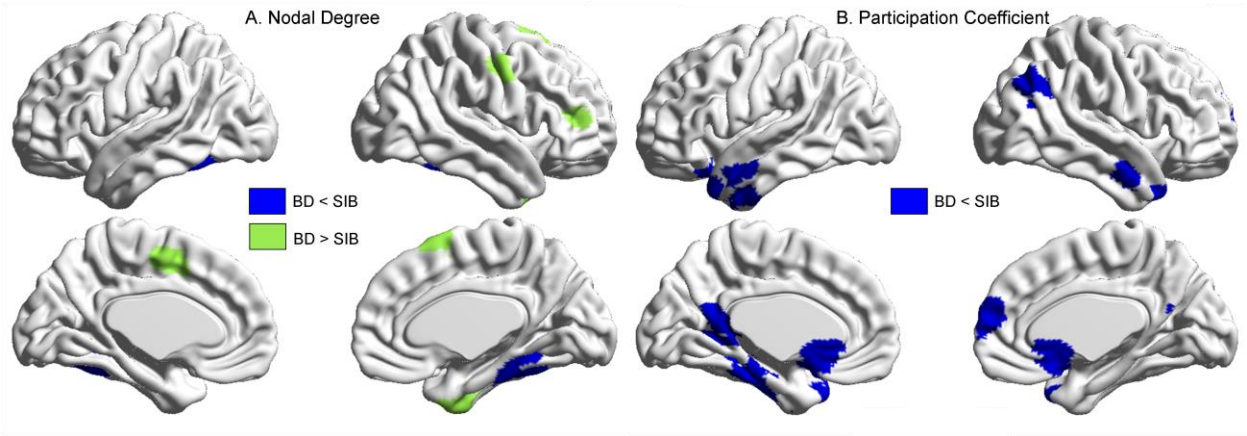

(A) Nodal degree; (B) Participation coefficient. Green: BD > SIB; Blue: BD < SIB; BD=patients with Bipolar Disorder; SIB=Siblings.

FIGURE S5. Average scores for the Barratt Impulsiveness Scale (BIS-11) sub-domains in each group.

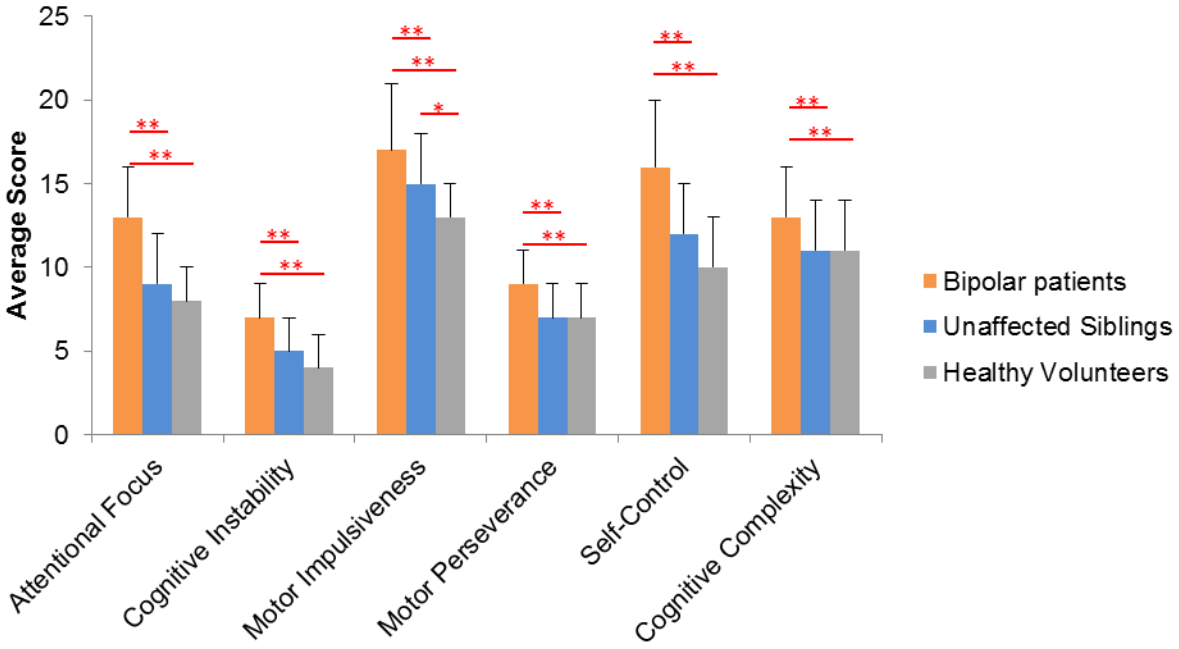

For each sub-domain, the ANOVAs showed significant group differences ($F \geq 22$; $p < 0.001$). For post hoc analyses: **: $p < 0.001$, Bonferroni corrected, *: $p = 0.004$, Bonferroni corrected. Error bars reflect standard deviation. The sub-domains 'Attentional focus' and 'Cognitive instability' are part of the 'Attentional' Factor; 'Motor impulsiveness' and 'motor perseverance' are part of the 'Motor' Factor; 'Self-control' and 'Cognitive complexity' are part of the 'Non-planning' Factor.

FIGURE S6. Results of the analyses testing the reliability of the results

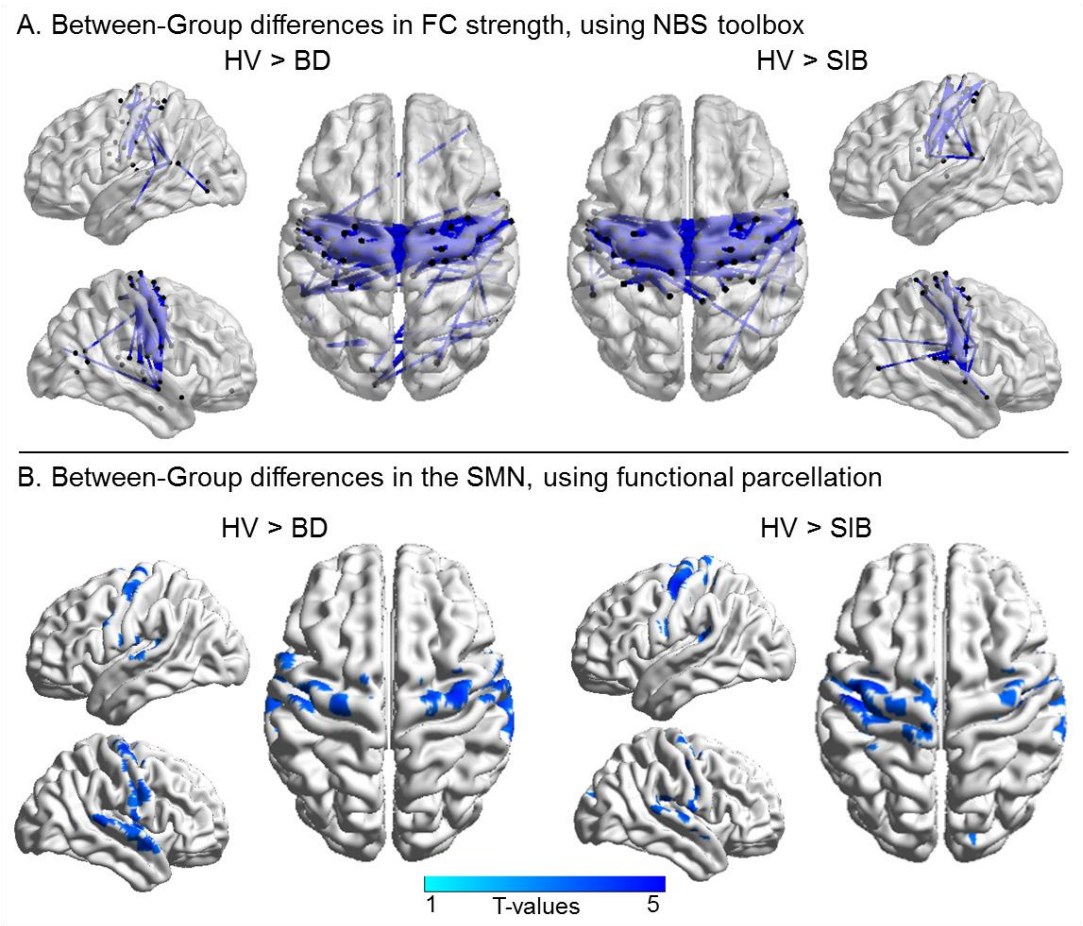

(A) Results of the t-tests on functional connectivity (FC) strength between the groups, showing reduced functional connectivity in the BD (left pannel) and SIB (right pannel) mostly involving nodes in the sensorimotor (SMN) and visual networks, relative to HV. Functional connectivity links with significant differences between the groups, at $p<0.05$, corrected for multiple comparisons (T-value ≥ 3.5; 5,000 permutations, based on the NBS toolbox). This results do not involve graph theory measures. (B) Results of the t-tests on the sensorimotor network (SMN) between the groups, based on dual regressions and the functional parcellation of the network provided by Shirer et al. (26). BD=patients with Bipolar Disorder; SIB=Siblings; HV=Healthy Volunteers; NBS= network-based statistic toolbox.

Supplemental References

1. First MB, Spitzer RL, Gibbon M, Williams JBW: Structured Clinical Interview for the DSM-IV-TR Axis I Disorders. Washington, DC, American Psychiatric Press; 2001.
2. Wechsler D: Wechsler Abbreviated Scale of Intelligence. San Antonio, CA, The Psychological Corporation; 1999.
3. Hamilton M. Development of a rating scale for primary depressive illness. The British journal of social and clinical psychology. 1967;6:278-296.
4. Young RC, Biggs JT, Ziegler VE, Meyer DA. A rating scale for mania: reliability, validity and sensitivity. The British journal of psychiatry : the journal of mental science. 1978;133:429-435.
5. Ventura J, Green MF, Shaner A, Liberman RP. Training and quality assurance with the Brief Psychiatric Rating Scale. International journal of methods in psychiatric research. 1993;3:221-244.
6. Goodwin FK, Jamison KR: Manic-Depressive Illness: Bipolar disorders and recurrent depression. 2nd ed. Press OU, editor. New York2007.
7. Kessler RC, Berglund P, Demler O, Jin R, Merikangas KR, Walters EE. Lifetime prevalence and age-of-onset distributions of DSM-IV disorders in the National Comorbidity Survey Replication. Archives of general psychiatry. 2005;62:593-602.
8. Song XW, Dong ZY, Long XY, Li SF, Zuo XN, Zhu CZ, He Y, Yan CG, Zang YF. REST: A Toolkit for Resting-State Functional Magnetic Resonance Imaging Data Processing. PloS one. 2011;6:e25031.
9. Cordes D, Haughton VM, Arfanakis K, Carew JD, Turski PA, Moritz CH, Quigley MA, Meyerand ME. Frequencies contributing to functional connectivity in the cerebral cortex in "resting-state" data. AJNR American journal of neuroradiology. 2001;22:1326-1333.
10. Tzourio-Mazoyer N, Landeau B, Papathanassiou D, Crivello F, Etard O, Delcroix N, Mazoyer B, Joliot M. Automated anatomical labeling of activations in SPM using a macroscopic anatomical parcellation of the MNI MRI single-subject brain. NeuroImage. 2002;15:273-289.
11. Crossley NA, Mechelli A, Vertes PE, Winton-Brown TT, Patel AX, Ginestet CE, McGuire P, Bullmore ET. Cognitive relevance of the community structure of the human brain functional coactivation network. Proceedings of the National Academy of Sciences of the United States of America. 2013;110:11583-11588.
12. Zalesky A, Fornito A, Harding IH, Cocchi L, Yucel M, Pantelis C, Bullmore ET. Whole-brain anatomical networks: does the choice of nodes matter? NeuroImage. 2010;50:970-983.
13. Guimera R, Amaral LA. Cartography of complex networks: modules and universal roles. Journal of statistical mechanics. 2005;2005:nihpa35573.
14. Latora V, Marchiori M. Efficient behavior of small-world networks. Physical review letters. 2001;87:198701.
15. Rubinov M, Sporns O. Complex network measures of brain connectivity: uses and interpretations. NeuroImage. 2010;52:1059-1069.
16. Joyce KE, Hayasaka S, Laurienti PJ. The human functional brain network demonstrates structural and dynamical resilience to targeted attack. PLoS computational biology. 2013;9:e1002885.
17. Albert R, Jeong H, Barabasi AL. Error and attack tolerance of complex networks. Nature. 2000;406:378-382.
18. van den Heuvel MP, Sporns O. Rich-club organization of the human connectome. The Journal of neuroscience : the official journal of the Society for Neuroscience. 2011;31:15775-15786.
19. Newman ME. Modularity and community structure in networks. Proceedings of the National Academy of Sciences of the United States of America. 2006;103:8577-8582.
20. Bassett DS, Porter MA, Wymbs NF, Grafton ST, Carlson JM, Mucha PJ. Robust detection of dynamic community structure in networks. Chaos. 2013;23:013142.

21. Good BH, de Montjoye YA, Clauset A. Performance of modularity maximization in practical contexts. Physical review E, Statistical, nonlinear, and soft matter physics. 2010;81:046106.
22. Gu S, Satterthwaite TD, Medaglia JD, Yang M, Gur RE, Gur RC, Bassett DS. Emergence of system roles in normative neurodevelopment. Proceedings of the National Academy of Sciences of the United States of America. 2015;112:13681-13686.
23. Cicchetti DV. Guidelines, criteria, and rules of thumb for evaluating normed and standardized assessment intruments in psychology. Psychological Assessment. 1997;6:284-290.
24. Hinkle DE, Wiersma W, Jurs SG: Applied Statistics for the Behavioral Sciences, Cengage Learning; 2006.
25. Zalesky A, Fornito A, Bullmore ET. Network-based statistic: identifying differences in brain networks. NeuroImage. 2010;53:1197-1207.
26. Shirer WR, Ryali S, Rykhlevskaia E, Menon V, Greicius MD. Decoding subject-driven cognitive states with whole-brain connectivity patterns. Cereb Cortex. 2012;22:158-165.
27. Team RC: R: A language and environment for statistical comuting. Vienna, Austria, R Foundation for Statistical Computing; 2015.
28. Xia M, Wang J, He Y. BrainNet Viewer: a network visualization tool for human brain connectomics. PloS one. 2013;8:e68910.
29. Leucht S, Kane JM, Kissling W, Hamann J, Etschel E, Engel R. Clinical implications of Brief Psychiatric Rating Scale scores. The British journal of psychiatry : the journal of mental science. 2005;187:366-371.